The Journal of Engineering

Research Article

IET Journals
The Institution of Engineering and Technology

Design, analysis, and realisation of chipless RFID tag for orientation independent configurations

eISSN 2051-3305
Received on 29th May 2019
Revised 10th August 2019
Accepted on 27th September 2019
E-First on 18th May 2020
doi: 10.1049/joe.2019.0920
www.ietdl.org

Mohammad S. Hashmi[1,2] ✉, *Vijay Sharma*[1]

[1]*School of Engineering and Digital Sciences, Nazarbayev University, Astana, Kazakhstan*
[2]*Electronics and Communication Engineering Department, IIIT-Delhi, New Delhi, India*
✉ *E-mail: mohammad.hashmi@nu.edu.kz*

Abstract: The architectures of two innovative compact orientation independent chipless radio frequency identification device (RFID) tags for emerging applications such as the internet of things are presented. These tags, when illuminated, generate resonant frequencies in the radar cross-section backscattered spectrum, which are used to encode the data. These are based around L-type resonators, which can be read from front and back using linear polarisation waves as they do not have the ground plane. The first tag design consists of L-resonators in the lower triangular of the substrate, and thereby mutual coupling is increased as a reduction in the size. The second tag design incorporates alternate L-resonators in both halves of the substrate and exhibits reduced mutual coupling and enhanced printing strength but with a reduction in bit density. The proposed concept is demonstrated through prototypes of 8-bit chipless tags on Rogers substrate. These tags require very low bandwidth to encode 8-bit and occupy a small board size of 20 mm × 20 mm, and these are considerable improvements in the development of chipless RFID.

1 Introduction

The radio frequency identification device (RFID) technology provides numerous benefits such as non-line-of-sight reading, extended reading range, increased data capacity, and automation in item tracking, identification, and localisation when compared to other approaches such as optical and radio frequency barcoding [1]. These exciting features make the RFID an important component for the broader internet of things (IoT) ecosystem [2, 3]. A typical RFID system, depicted in Fig. 1, includes two key elements, namely the tag which transmits encoded data over a wireless medium and the reader that queries remotely placed tag and then decodes the received signal [4]. Primarily, the plane wave generated by the reader excites the tag at some distance which gets modified based on the encoded data in the tag and transmits back information to the reader. The reader decodes a unique ID from the received response and then sends that to the database for verification.

However, a major hindrance to the wide applicability of RFID systems is the presence of the silicon microchip in the tag which increases the cost and fabrication complexity. To address these concerns, the development of chipless RFID tags have been reported [5]. These are inexpensive and readily printable and therefore possess the potential for cost-effective mass production to facilitate the deployment in emerging applications such as IoT. The chipless RFID tags encode data in the form of the electromagnetic footprint of the tag [6].

In general, the chipless RFID tags can be categorised into two distinct groups, depending on their respective spectral signatures, the retransmission type [7], and the backscattering type [8, 9]. The retransmission type tags capitalise on multiple antennas for communication between the reader and the tag. The antennas allow the tag to be read from a longer distance. However, this adds to the size and, therefore, the cost of the tag [10]. The backscattering type tags modulate the query signal and scatter it in the same direction as the query signal [11]. The backscattering type tags can be designed significantly smaller in size when compared to retransmission type tags under similar frequency and operating conditions [12, 13] and, therefore, could be potentially more appropriate for IoT applications. There have been several reports that have subsequently advanced the chipless RFID technology [14, 15].

The chipless RFID tag utilising shunt capacitors [16] enables easy printing but suffers from increased size as the number of encoded bits increase. Other design reports such as dipoles based [17], and multiple quarter wavelength slot-based [18] also suffer from increased size. The dipole-based tag is also extremely limited in the reading range. The alternative space-filling curve type chipless tag seems very exciting, but this technique inherently introduces complexity in design, fabrication, and encoding of data [19]. Furthermore, a chipless tag with stub-loaded patch antennas enables the encoding of bits in the phase domain [20]. However, the encoding of data in the phase often suffers from multipath effect. There has been a recent emphasis on the chipless tags employing the backscattering concept [11, 21, 22]. However, the major constraints in these designs are the requirements of large bandwidth, orientation independence, and higher frequencies for the encoding of data [23].

Overall, it is safe to mention that there is an urgent need to address the issues such as larger tag size, the requirement of large bandwidth etc. usually present in the existing chipless RFID tag design techniques. It is also pertinent to note that the chipless tag design technique addressing these issues can be extremely useful and will have the potential to gain wide acceptance in emerging applications such as the broader IoT framework. Therefore, this study proposes the architectures of two orientation independent (OI) chipless RFID tags to addresses several of the identified concerns. In essence, the chipless tags can be analysed with the help of a plane wave, linearly polarised antennas or waveguides and the size of the tags does not increase linearly with an increase in the number of bits. The most important features of the presented designs include simple printability, orientation independence, small bandwidth, small tag size, and precise readability from back and front. This places them in an ideal position for various IoT applications including tagging and identification of items such as in the supermarkets, warehouses, tracking of drugs and blood bank inventory etc. In Section 2, the theoretical foundation is laid out for the designs. Section 3 provides the details about the prototypes developments whereas Section 4 provides elaborated discussion on the measurement and validation. Section 5 describes a detailed

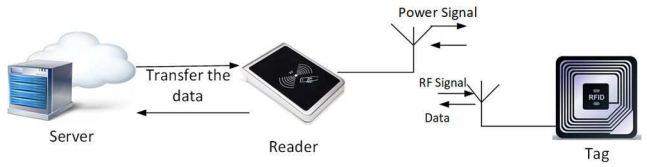

Fig. 1 *General RFID system*

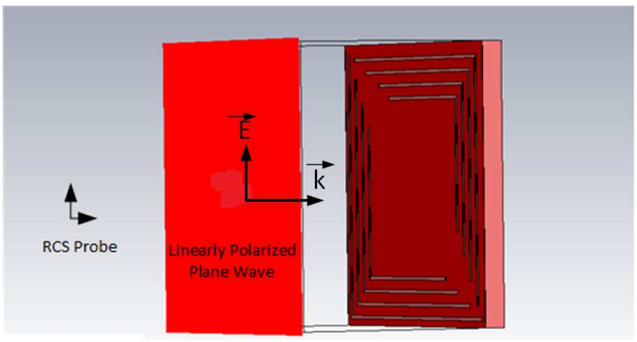

Fig. 2 *CST microwave studio simulation setup for the investigation of tag and resonator capabilities*

analysis of the design strategy, measurements, and performance evaluation is provided.

2 Resonator design

2.1 Theory of L-shaped resonators

A plane wave having linear polarisation is incident on a single bit L-resonator to investigate the properties of the L-resonator. The wave is incident normal of the surface of the resonator. The respective directions of the E-field ($\boldsymbol{E}$) and plane wave ($\boldsymbol{k}$) are shown in Fig. 2. In the L-resonators, the length and their respective resonant frequencies are related as in [24]

$$f = \frac{c}{2L_x}\sqrt{\frac{2}{\varepsilon_r + 1}} \tag{1}$$

where c is 3×10^8, ε_r is the relative permittivity of the substrate, and L_x represents the xth resonator length.

It is apparent from (1) that a number of distinct resonant frequencies can be realised by resonators of varying lengths. This can eventually allow encoding of unique data on each resonator as they possess unique frequency signatures. In essence, the presence of an L-resonator symbolises a '1' and the unavailability of L-resonator indicates a '0'. To understand this aspect, a simulation has been carried out for an L-resonator operating in the traditional ultra-wideband frequency range. In this context, Fig. 3*a* depicts a typical resonator at a frequency of 3.1 GHz according to (1). It can be seen in Fig. 3*c* that this resonator exhibits repetitive resonating feature beyond 8 GHz and therefore is safe for unique encoding between 3 and 8 GHz. For example, an 8-bit RFID tag using the L-resonators can be realised within a window of 3–6 GHz without encountering the issue of repetitive resonance.

The design of resonators can also be understood by looking through the surface current density variations along its dimensions in Fig. 3*b*. Apparently, it depicts good radiating features at the resonating frequency. This aspect of current density dependence on the dimensions of the resonator can also be analysed using (2) [25]

$$J = \frac{-E_0}{2\pi f \mu}\sqrt{k^2 - \left(\frac{\pi}{L_x}\right)^2}\sin\left(\frac{\pi x}{L_x}\right)e^{-j\sqrt{k^2-(\pi/L_x)^2}z} \tag{2}$$

where f is the resonating frequency, k is the wave number, E_0 is the constant power given to the resonator, L_x is the length of the xth resonator, and μ is the material's permeability.

The relationship between the surface current density (dBA/m) and the length of the L-resonator (mm) has been highlighted in

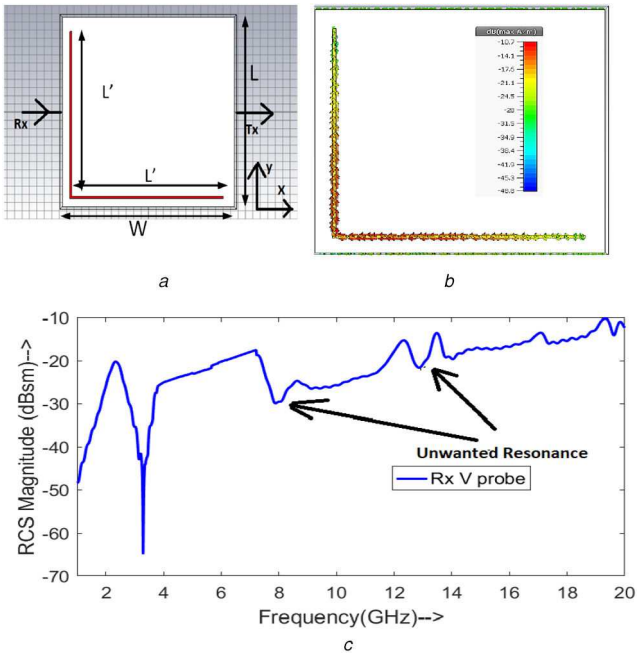

Fig. 3 *Demonstration of performance of single bit resonator*
(a) Single bit L-resonator, ***(b)*** Magnitude of surface current density, ***(c)*** Magnitude response of RCS of one bit L-resonator at 3.1 GHz

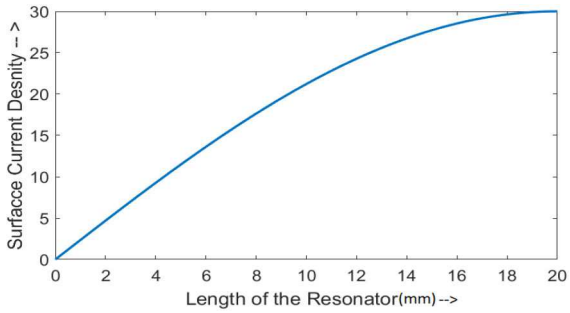

Fig. 4 *Values of surface current density around the resonator*

Fig. 4 using (2). Now for the specific values of $z = 0$ (surface current is a planner), $L = 38$ mm, $f = 3.1$ GHz, $\mu = 1$, $k = 2\pi/bda$ and $E_0 = 1$ mW, the value of x is varied from 0 to 20 mm to obtain the variations in Fig. 4. The parameter x only corresponds to one edge of the L-resonator. Apparently, the simulated and analytically obtained current density variations show an identical dependence. It is also imperative to note that the sensitivity of the reader depends on the surface current density. Therefore, Fig. 3 can also enable the determination of tags dimensions for any specified application.

2.2 Reading mechanism in backscattering chipless tags

The interrogation signal illuminates the tag and reflects after modifying it according to the information in the tag. The reader is highly directive, and therefore the intensity of the signal is in the direction of the tag. Here, the illumination angle of the reader has been kept fixed. The performance is measured, as discussed in Sections 4 and 5, at different orientations of the chipless tag. The overall process is depicted in Fig. 5. Furthermore, the backscattered signal has the encoded bits in the frequency domain, and this information is decoded in the reader.

In such a system, the magnitude of radar cross-section (RCS) is measured using (3) [26]

$$\sigma = \lim_{r \to \infty} 4\pi r^2 \frac{|E_{scat}|^2}{|E_{inc}|^2} \tag{3}$$

where E_{inc} and E_{scat} denote the incident and scattering electric field, respectively, on the tag, and r is the distance between the antenna and tag.

Moreover, in such a system, only a backscattered signal generated from the scattering of the tag by a wave having linearly polarised carries the information, and the response is recorded at the receiver (Rx) end of the RFID reader. The transmitter (Tx) and Rx system antennas need to be of similar polarisation for the precise study of the remotely placed tag and should have appropriate separation to avoid interference. The absence of ground also allows the chipless RFID tags to be OI as it can be read from front and back depending upon the RX antenna position. So, the OI tags can be read using a set of linearly polarised antennas or waveguides.

3 Tag design approach

In this study, prototypes of two distinct 8-bit chipless RFID tags operating in 3–6 GHz utilising L-resonators discussed in Section 2 are reported. The chipless tags have been designed using CST Microwave Design Studio and printed on the Roger RT 5880 substrate. The properties of the substrate are $\varepsilon_r = 2.2$, and height $(h) = 1.575$ mm. To ease the process of fabrication, the length of the patch resonators and the distance between individual resonators have been kept uniform. The in-house production also constrained the width of resonators to 0.25 mm as anything below this was not feasible. The respective parameters obtained using (1) for the chosen substrate for both the proposed designs are given in Table 1. There is a small shift in the length of the L-resonator at the time of final optimisation as compared to simulated values.

3.1 Design of first tag

One of the motivations in the design of the chipless RFID tag is the design simplicity and easy printability. Keeping these aspects in perspective, the width of L-resonators and gap between the resonators are placed the same equal to 0.25 mm. The corresponding lengths of the L-resonators are determined from (1). In this case, the L-resonators to realise the 8-bit tag have been placed on the substrate in one half of the board as shown in Fig. 6*a*. A plane wave having linear polarisation will elicit an RCS response from this structure and an RCS probe placed in the far-field will record this backscattered response. A reader can then decode an 8-bit unique ID from the recorded response as shown in Fig. 6*b*.

In the frequency signature, Fig. 6*b*, the longest resonator corresponds to the most significant bit, while the smallest resonator is designated for the least significant bit of the encoded data. The presence of a frequency signature will be denoted by a '1' and the absence by a '0'. The resonator-based chipless tag exhibits characteristics similar to a wideband antenna. The availability of more advanced printing tools can enable incorporation of more resonators and hence encoding of more number of bits without increasing the tag size. In any case, the increase in the number of bits will not lead to a linear increase in size. For the chosen example of 8 bits, the tag size is 20 mm × 20 mm, and this readily fulfils the need for miniature tags for applications such as IoT. However, in this design, the close proximity of the resonators to one another has the potential to affect the overall performance due to the mutual coupling which may lead to problems in the precise reading of the tag. The other apparent limitation could be its scalability.

3.2 Design of second tag

Another design for a similar set of frequencies as the first design is shown in Fig. 7*a*. Here, the odd-numbered resonators occupy lower triangular half of design while the even numbered are in the upper triangular of the design. Once again, the lowest frequency corresponds to the longest resonator in the tag, whereas the shortest resonator gives a frequency signature at the highest frequency. The presence or absence of resonators signifies a '1' or '0', respectively. The distance between strips is more in the second

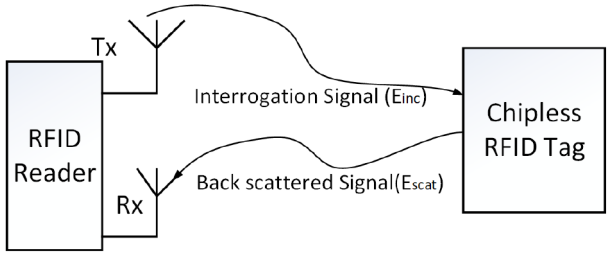

Fig. 5 *Depiction of reading technique in backscattered chipless RFID systems*

Table 1 Structural parameters for the proposed OI chipless tags having 8-Bit (from Fig. 3)

Parameter, s	Value, mm
chipless tag length, L	20
chipless tag width, W	20
the entire length of lengthy L-resonator $(L_1) = 2 \times L'$	38
length of consecutive resonators (L_{x+1})	$L_x - 2.78$
width of L-resonators	0.25
first design inter-resonator gap	0.25
second design inter-resonator gap	0.5

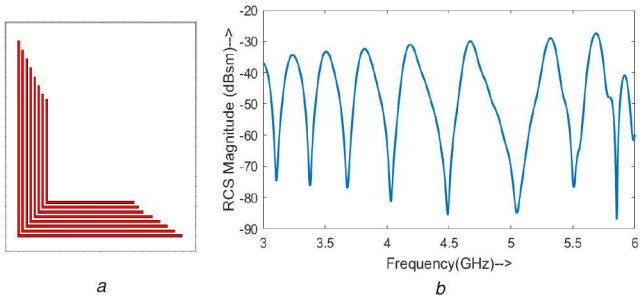

Fig. 6 *First 8-bit proposed chipless RFID tag*
(a) Tag design, ***(b)*** Simulated response of RCS

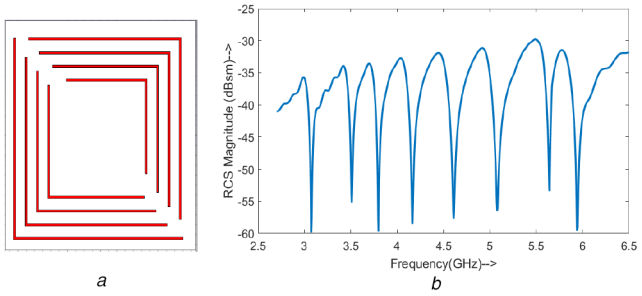

Fig. 7 *Second 8-bit proposed chipless RFID tag*
(a) Tag design, ***(b)*** Simulated response of RCS

design as compared to the first tag, which causes the narrowband resonances in nature, Fig. 7*b*, as compared to the first design and, therefore, can facilitate more accurate decoding of tag data.

Furthermore, the narrow resonance enables the encoding of a number of bits in a similar frequency range. This design also mitigates the effect of mutual coupling in comparison with the first design considering the larger gap between the resonators. Considering all of these exciting features, this design can be potentially useful for dense IoT applications. However, the size of this design will increase substantially with the increasing number of bits.

4 Study and discussion of the L-resonator-based chipless tags

To further examine the characteristics of the proposed L-resonator-based chipless tag, various simulations are performed using CST

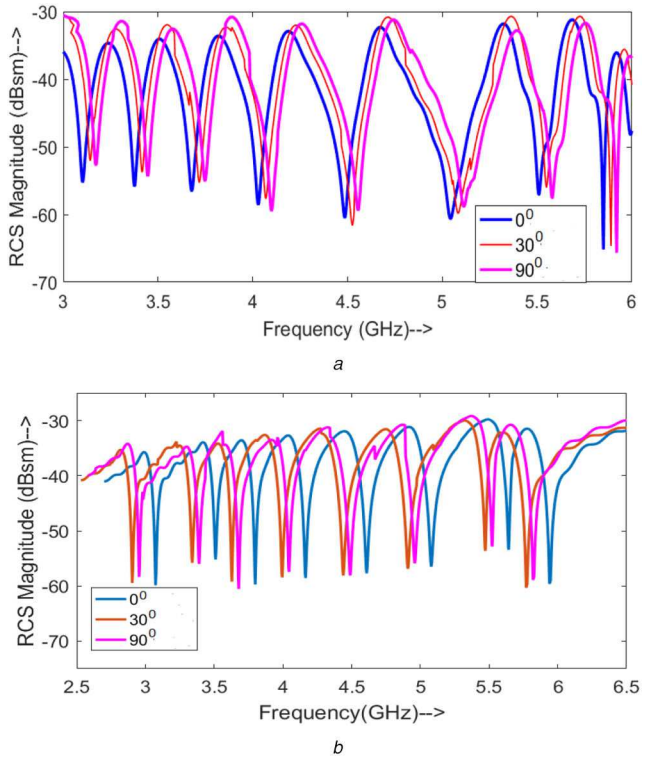

Fig. 8 *RCS magnitude response at the orientation of 0 °, 30 °, and 90 °*
(a) First tag, ***(b)*** Second tag

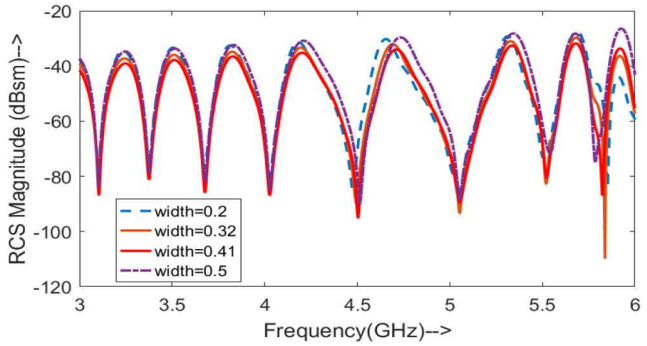

Fig. 9 *RCS response for varying resonator widths of the proposed chipless tag*

microwave studio. Here, a plane wave having linear polarisation is incident on the tag, discussed in Section 2.1, and a far-field probe is located at a length of 80 mm to collect the backscattered signal from the chipless tag. Then the impact of substrate characteristics, gaps between the L-resonator, the arrangement of the RCS Rx, and the ground plane on the efficiency of the tags have been studied and explained.

4.1 Effect of tag orientation

This is an extremely important feature for any RFID tag as it can be useful for important applications such as tagging of items in a supermarket or a sensor in the IoT framework. Such applications can be aided to a great extent by OI tags. It is due to the fact that these applications may have tags in any orientation and still need to be read accurately. To discuss the orientation independence of both the tags, a simulation framework was developed to assess the RCS magnitude at various orientations of the tags in CST software. The outcomes for orientations of 0 °, 30 ° and 90 ° are depicted in Figs. 8*a* and *b*. The simulation results show small shifts of ∼100 MHz on the first tag and around 300 MHz on the second tag, in the resonant frequencies under all the orientation in the worst case scenario. However, these shifts do not adversely affect the reading ability from the tags considering that the sharpness and narrowband feature of the signatures remain intact. Additionally, such minor

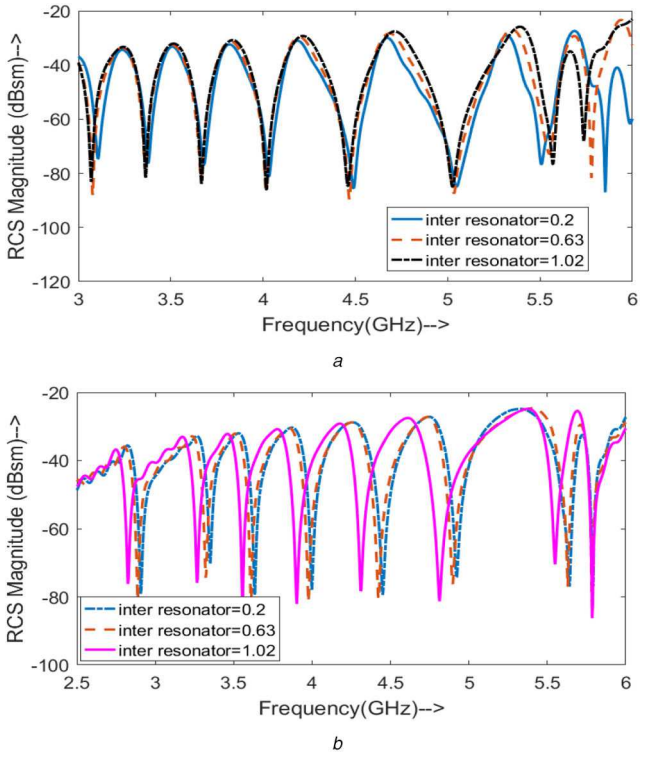

Fig. 10 *Effect of varying inter-resonator gap*
(a) RCS response of the first tag, ***(b)*** RCS response of the second tag

shifts can be readily calibrated in the reader using a correction algorithm or compensation factor [27, 28] for enhancing the readability of the tags.

4.2 Effect of resonator width

It was mentioned earlier that a remote printing facility constrained the choice of dimensions and gaps. The resonator width is one such limitation. However, some applications may require more compact and densely encoded tags, and this requires an understanding of the dependence of tag performance on resonator width. In this context, Fig. 9 shows RCS response for multiple widths, within a practical limit, of the resonator while keeping a fixed tag size. It can be inferred from this plot that although the sharpness in the notch gets enhanced with the decrease in resonator widths, the quality of reading will not be affected significantly. Moreover, narrow width resonators lead to a higher number of encoding bits within the same size of tags. This can facilitate features such as security within the tags. However, compact designs require sophisticated printing resources and can escalate the tag cost. It is imperative to note that the practical limit for the selection of widths can be dependent on several factors such as the required tag size, printing facility, desired applications etc.

4.3 Impact of inter-resonator gap

The inter-resonator gap is another constraint imposed by the in house printing resource. Mutual coupling between L-resonators decreases as the gap between L-resonators is increased. This result decreases the inductance between two L- resonators. This effect clearly indicates in Figs. 10*a* and *b* as decreased inductance shifts the frequency resonances to the right. The shifts in the resonances are more remarkable in the second chipless tag design, as L-resonators are present on both upper and lower triangular of the substrate which leads to more reduction in the mutual coupling compared to the first chipless tag design. However, the tag readability is not affected by the variations in these gaps as the sharpness of the resonance persists. It is important to note that the smaller inter-resonator gaps lead to increased coupling and the larger gaps will lead to increased size. Therefore, depending on the application, a trade-off can be made to choose the inter-resonator gaps.

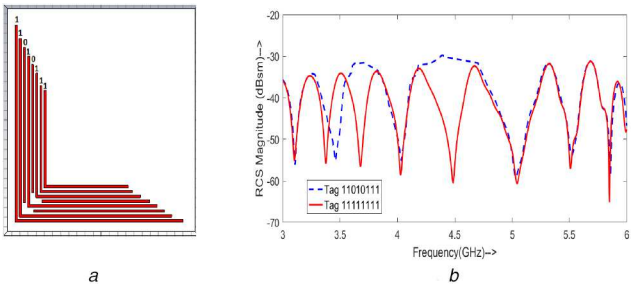

Fig. 11 *Investigation and demonstration of bit encoding in first tag*
(a) Structure of the first tag for the encoding of '11010111', ***(b)*** Depiction of the original and modified RCS responses

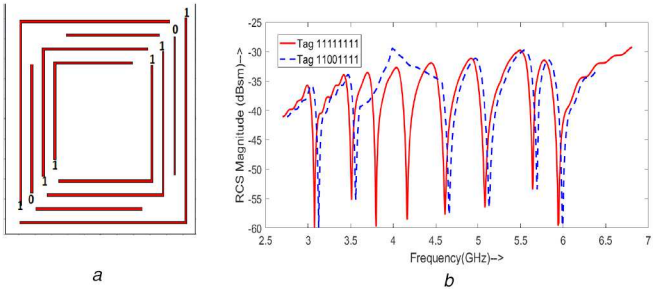

Fig. 12 *Investigation and demonstration of bit encoding in second tag*
(a) Structure for the encoding of '11001111', ***(b)*** Depiction of the original and modified RCS responses of the second tag

4.4 Data encoding mechanism

It has been shown that the presence of resonant frequencies within the specified band is identified by '1'. Apparently, a slight change in the design of resonators can enable the encoding of '0'. For example, in the first tag, shown in Fig. 11*a*, the third and fifth resonators are etched from the origin.

The corresponding frequency signatures of both the original and modified designs are depicted in Fig. 11*b*. It is apparent that the modified tag does not exhibit resonant frequencies for the third and fifth resonators within the specified range of frequencies of 3–6 GHz. The absence of the resonant frequencies, therefore, enables the encoding as '11010111'.

Similarly, the second tag can also be restructured for the encoding of desired bits. For example, the encoding of '11001111' requires etching of third and fourth resonators from the origin as shown in Fig. 12*a*. It is clear from the frequency signature of the modified tag, given in Fig. 12*b*, which does not exhibit resonance for the third and fourth resonators in the given frequency band of 3–6 GHz. Therefore, it can be encoded with '11001111'.

4.5 Impact of the ground plane

It has been demonstrated that the proposed tags, an absence of ground plane, can be encoded from both sides (front and back). To investigate this interesting property, the ground plane has been introduced on one side of the tag. The RCS responses of the original and modified tags, while measuring from the front, are depicted in Fig. 13. The ground plane acts as a mirror and enhances the field strength. It is apparent that the power level of the received signal in a design with no ground plane is better compared to the design having a ground plane. This can definitely lead to a more accurate reading of the tag with no ground. Ground plane also decreases the influence of substance or object where the tag is attached. Moreover, the presence of the ground plane means that the tag no longer scatters in both directions and that will put a limitation on the reader's placement.

It is important to note that tags of both types, with ground and without ground, are required depending on the application scenario. In this context, tags with no ground can be required in applications such as personal identity cards, while applications requiring security such as bank cards might find the usefulness of tags with the ground.

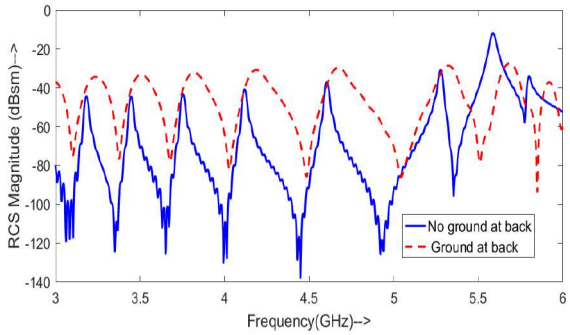

Fig. 13 *RCS response for the presence and absence ground plane of proposed chipless tags*

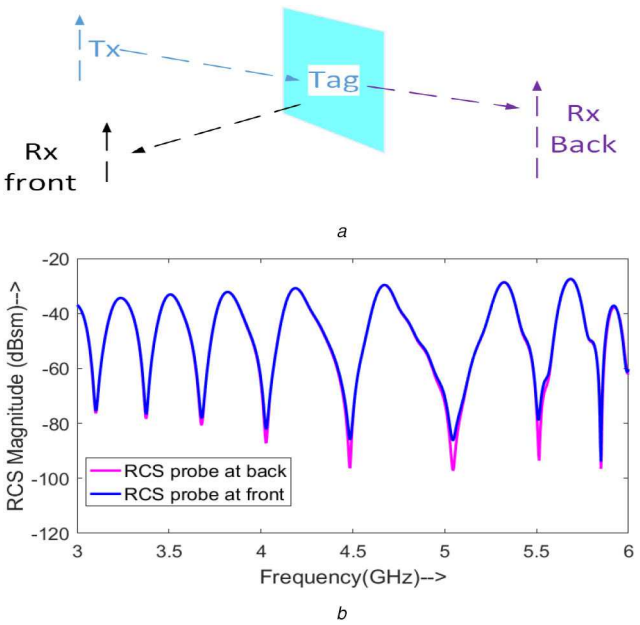

Fig. 14 *Investigation and demonstration of tag reading ability*
(a) Placement of RCS Rx probe on both sides of the tag, ***(b)*** Simulated RCS magnitude responses on different positions of the probe

4.6 Impact of Rx probe placement

Some applications may require the reading of the tags from either front or back. To investigate the readability of tags, the probes are placed at the front and back as shown in Fig. 14*a*. The obtained results for both the scenarios are shown in Fig. 14*b*. This is clear that the responses are in perfect agreement in terms of resonant frequencies and power levels. This conveys that the reading from both sides will be the same and accurate.

4.7 Impact of substrate properties

The chipless tags will be printed on items with differing relative permittivities and substrate heights. This will lead to changed resonant frequencies as can be seen in Fig. 15. The RCS response for three common materials with varying dielectric materials shows that the resonant frequency shifts to the left with an increase in dielectric constant and it is in consonance with (1). In practical applications, it might lead to situations when the dimensions of the resonators will require some tweaking to encode desired bits within the chosen frequency range. The apparent impact of this will be the closer resonant frequencies and hence the possibility of an incorrect reading of the tag in the worst case scenario.

Furthermore, it can also be seen that the paper substrate with a height of 0.1 mm can also provide the possibility of the desired encoding of bits. It will effectively provide a very cost-effective solution. However, the signal strength is quite low as compared to other lossy substrates, and therefore reader with very high sensitivity will be required to read the backscattered signal from the paper substrate tag.

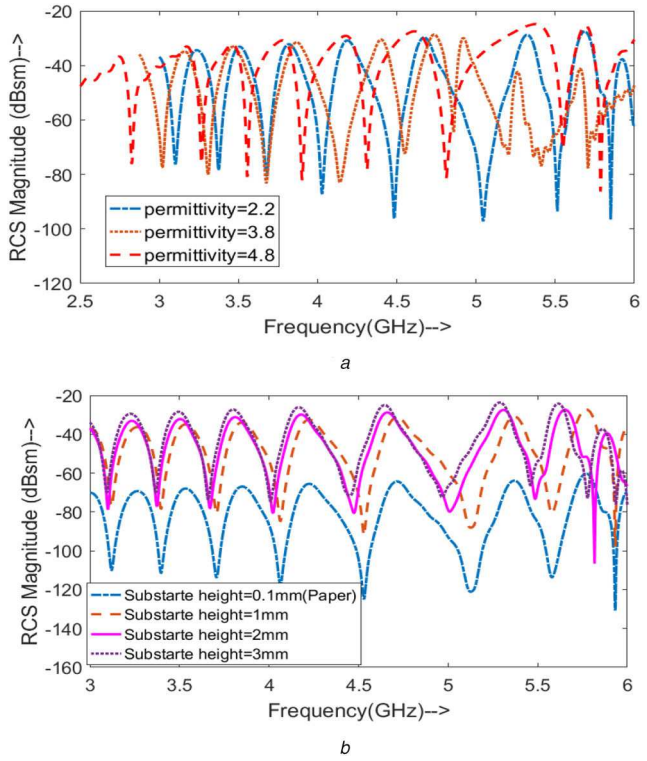

Fig. 15 *RCS responses for chipless tags having*
(a) Different dielectric properties, ***(b)*** Different substrate heights

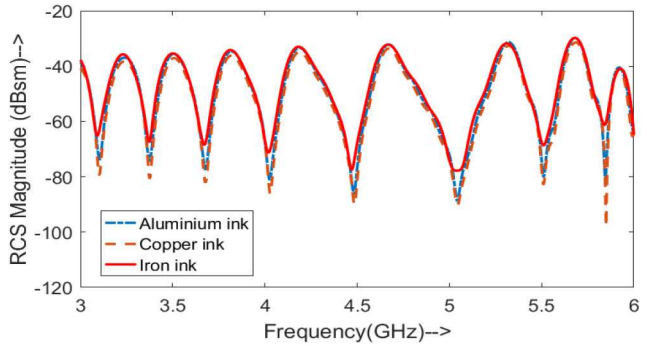

Fig. 16 *RCS response with different metallic layers on the proposed tags*

4.8 Impact of various metal layers

The chipless tag models were fabricated on a Rogers substrate having a copper layer of conductivity of 5.8×10^7 S/m. The mass deployment of such tags necessitates a cost-effective solution. To understand the effectiveness of the proposed technique, an additional simulation was carried out with aluminium (conductivity = 36.9×10^6 S/m), and iron (conductivity = 10.1×10^6 S/m). The RCS responses under these varying scenarios depicted in Fig. 16 demonstrate that the proposed designs can work appropriately on relatively low-cost material having iron as the conductive ink.

5 Results and discussion

5.1 Measurement setup

The measurement setup used to validate the performance of tags is depicted in Fig. 17. Here, two linearly polarised horn antennas with bandwidths of 1–15 GHz and gains of 9 dBi are used for analysing the proposed chipless RFID tags. The Tx/Rx system of antennas in the experiment works such as a bistatic radar system where one antenna is used to interrogate the target (which are the chipless tags), and another antenna is used to receive the scattered signal from the target. The tags scatter the linearly polarised wave in both the front and back directions as they do not contain a ground plane.

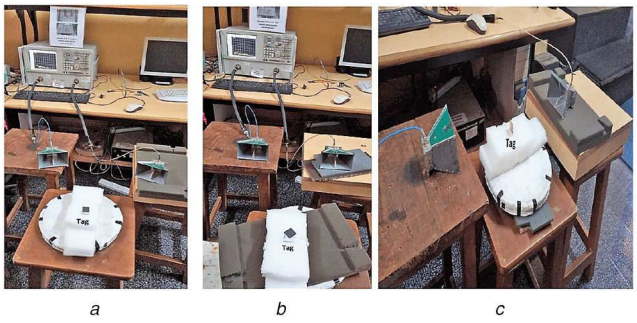

Fig. 17 *Evaluation setup inside the lab*
(a) When the tag is on the same side of antennas, ***(b)*** When the tag is placed at 45 °, ***(c)*** When the tag is on the opposite side of the tag of antennas

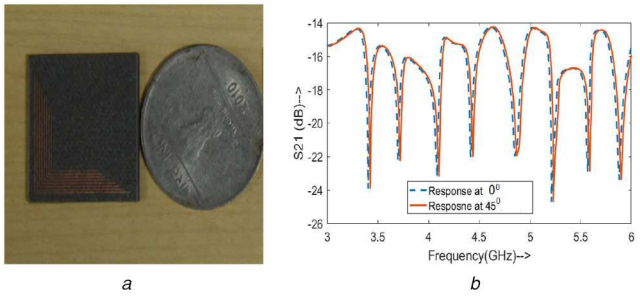

Fig. 18 *First 8-bit proposed chipless RFID tag*
(a) Fabricated design, ***(b)*** Measured response of S_{21} when the tag is on the same side of antennas

For proof of concept, the measurements were carried out under different setup configurations in a room environment. In the initial, the antenna has been calibrated according to the environment of the room. It removes the noise and interference because of the antennas and other materials at the time of measurements of tags. In the first chipless RFID configuration, both the horn antennas were placed in front of the tags as shown in Fig. 17*a*, while the configuration in Fig. 17*b* had antennas in front but with 45 ° orientation. In both these cases, the antennas are placed 45 cm further from the chipless tag while both these antennas are kept 40 cm apart from each other to minimise interference. In the last configuration, in Fig. 17*c*, the linearly polarised horn antennas are arranged on opposite sides of the tags. In all experiments, the height of the position of the tag and height of the Tx and Rx antennas are kept the same. A vector network analyser transmits 30 dBm (1 W) power through port 1, and subsequently, the transmission coefficient (S_{21}) is measured.

5.2 Performance evaluation of first chipless tag design

The chipless RFID tag, displayed in Fig. 18*a* was fabricated as per the architectural parameters in Table 1 to operate in the frequency band of 3–6 GHz. The recorded performance in terms of S_{21} is depicted in Fig. 18*b*.

It is clear from the measured S_{21} profile, in Fig. 18*b*, that eight particular frequency resonances are present in the 3–6 GHz band and essentially denote the encoded 8-bit '11111111'. These are marked with a dotted line. To illustrate the orientation independence nature, the chipless tag is turned by 45 °. The obtained results, indicated by a solid line in Fig. 18*b*, show nominal shifts in the frequency signatures and thus validate the orientation independence. Actually, the nominal deviation in the resonant frequencies can be promptly corrected in the RFID reader.

5.3 Performance evaluation of second chipless tag design

The second chipless RFID tag design demonstrated in Fig. 19*a* is also prototyped using the architectural parameters in Table 1. Once again the chosen frequency range is 3–6 GHz. As mentioned earlier, this design includes the odd numbered L-resonators in lower triangular of the board whereas the even-numbered L-

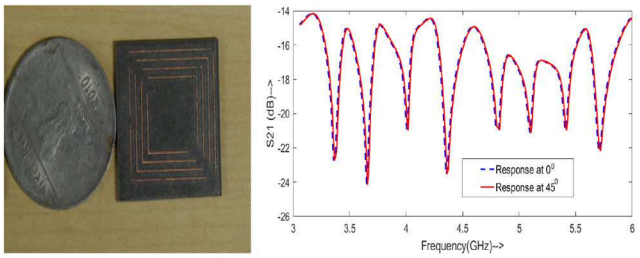

a b

Fig. 19 *Second 8-bit proposed chipless RFID tag*
(a) Fabricated design, ***(b)*** Measured response of S_{21} when the tag is on the same side of antennas

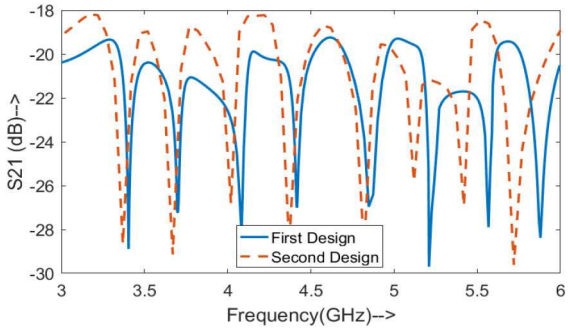

Fig. 20 *Measured magnitude S_{21} response of both the proposed designs of chipless RFID when Tx and Rx reader antenna are on the opposite side of the tag*

Table 2 Comparison with an existing chipless tag on different parameters

Chipless RFID types	Bit density (bits/cm^2)	Printable	Size increment with bits	OI	Bandwidth requirement	No. of Bit encoded
Surface Acoustic Wave [29]	>1.0	no	yes	yes	N/A (time and phase shifting tag)	64
stub-loaded microwave patch antenna [20]	0.18	yes	yes	no	0.5 GHz	3
C-phase tag [22]	2.88	yes	yes	no	5 GHz	22.9
Time Domain Reflectometer [16]	0.17	yes	yes	no	N/A	N/A
coplanar [30]	3.3	yes	n/a	no	3.5 GHz	N/A
Chipless RFID [31]	3.56	yes	yes	no	7.5 GHz	28.5
c-like [32]	0.90	yes	yes	no	3.5 GHz	19.9
c resonators [33]	1.14	yes	yes	no	2 GHz	20
compact orientation tag [13]	N/A	yes	yes	yes	7 GHz	8
this paper	>4.0	yes	no	yes	3 GHz	8

resonators are in inverted fashion in the upper triangular. Apparently, eight unique frequency signatures in the S_{21} response, marked using a solid line in Fig. 19*b*, arise, and they denote the encoded 8-bit '11111111'. To demonstrate the orientation independence nature of the proposed tag, the chipless tag is rotated by an angle of 45 °, and the results are presented using a dashed line alongside the original S_{21} results in Fig. 19*b*. In both these situations, the tag is on the same side of the antennas. A good agreement between the signatures demonstrates the orientation independence of the tag. In any case, the minor shifts in the resonant frequencies can be corrected in the reader.

To show the reading ability from the tags, the experiment was performed while keeping one antenna each in the front and back of the tags. The measured S_{21} magnitude response, given in Fig. 20, for both the chipless tags in such a situation, demonstrates the effectiveness of the proposed designs. It is apparent that the S_{21} responses are sharp in a narrow bandwidth and, therefore, can promote the encoding of desired 8-bit.

In summary, it can be inferred that the resonant frequencies of the proposed designs slightly shift with the changes in relative permittivity, substrate height, inter-resonator gap, and Rx location. However, these shifts are minor and can readily be calibrated in the reader. Moreover, for a cost-effective mass deployment, the tags can be printed on a paper substrate using highly conductive ink to improve the magnitude of the resonant notches for accurate reading of the tags. It provides a very high-density of 4 bits/cm^2. Overall, the choice of all these parameters will be regulated by the application space within the broad spectrum of IoT applications.

Finally, the comparison has been done on the basis of different properties of the proposed chipless tags with the existing literature in Table 2. It is clear that the proposed chipless tags designs exhibit the desired features such as orientation independence in addition to high-bit density. The significantly enhanced features make the proposed designs an excellent candidate for emerging IoT applications.

6 Conclusion

Novel designs of two OI chipless RFID tags with significantly enhanced performance over the existing designs have been proposed in this study. The orientation independence in the designs is inherent and is the outcome of the appropriate placement of the L-resonators. The proposed tags exhibit exciting features such as printability, low bandwidth, high bit density, miniature size and readability from back and front in addition to orientation independence. All these features have been analysed in simulation and demonstrated experimentally. Furthermore, it has been shown that the designs could be a potential candidate for cost-effective mass deployment solutions if some features can be traded-off.

7 Acknowledgment

The authors would like to thank Prof. K.J. Vinoy, IISc Bangalore for providing the facilities and guidance for measurements of the tags.

8 References

[1] Popperl, M., Adametz, J., Vossiek, M.: 'Polarimetric radar barcode: a novel chipless RFID concept with high data capacity and ultimate tag robustness', *IEEE Trans. Microw. Theory Tech.*, 2016, **64**, (11), pp. 3686–3694
[2] Preradovic, S., Balbin, I., Karmakar, N.C., *et al.*: 'A novel chipless RFID system based on planar multiresonators for barcode replacement'. IEEE Int. Conf. on RFID, Las Vegas, NV, USA, April 2008, pp. 289–296
[3] Valhouli, C.A.: 'The internet of things: networked objects and smart devices'. The Hammersmith Group Research Report, vol. 20, 2010
[4] Bibile, M.A., Karmakar, N.C.: 'Moving chipless RFID tag detection using adaptive wavelet based detection algorithm', *IEEE Trans. Antennas Propag.*, 2018, **66**, (6), pp. 2752–2760
[5] Preradovic, S., Karmakar, N.C.: 'Design of fully printable planar chipless RFID transponder with 35-bit data capacity'. European Microwave Conf. (EuMC), Rome, Italy, 2009, pp. 013–016
[6] Feng, C., Zhang, W., Li, L., *et al.*: 'Angle-based chipless RFID tag with high capacity and insensitivity to polarization', *IEEE Trans. Antennas Propag.*, 2015, **63**, (4), pp. 1789–1797
[7] Sharma, V., Hashmi, M.: 'Chipless RFID tag based on open-loop resonator'. IEEE Asia–Pacific Microwave Conf. (APMC), Kuala Lumpur, Malaysia, November 2017, pp. 543–546

[8] Preradovic, S., Karmakar, N.C.: 'Chipless RFID: bar code of the future', *IEEE Microw. Mag.*, 2010, **11**, (7), pp. 87–97
[9] Khaliel, M., El-Awamry, A., Megahed, A.F., *et al.*: 'A novel design approach for co/cross-polarizing chipless RFID tags of high coding capacity', *IEEE J. Radio Freq. Identif.*, 2017, **1**, (2), pp. 135–143
[10] Betancourt, D., Barahona, M., Haase, K., *et al.*: 'Design of printed chipless-RFID tags with QR-code appearance based on genetic algorithm', *IEEE Trans. Antennas Propag.*, 2017, **65**, (5), pp. 2190–2195
[11] Islam, M.A., Karmakar, N.C.: 'Compact printable chipless RFID systems', *IEEE Trans. Microw. Theory Tech.*, 2015, **63**, (11), pp. 3785–3793
[12] Wang, L., Liu, T., Sidén, J., *et al.*: 'Design of chipless RFID tag by using miniaturized open-loop resonators', *IEEE Trans. Antennas Propag.*, 2018, **66**, (2), pp. 618–626
[13] Sharma, V., Malhotra, S., Hashmi, M.: 'Orientation independent printable backscattering chipless RFID tags based on l-resonator'. 48th European Microwave Conf. (EuMC), Madrid, Spain, September 2018, pp. 989–992
[14] Havlicek, J., Svanda, M., Polivka, M., *et al.*: 'Chipless RFID tag based on electrically small spiral capacitively loaded dipole', *IEEE Antennas Wirel. Propag. Lett.*, 2017, **16**, pp. 3051–3054
[15] Polivka, M., Havlicek, J., Svanda, M., *et al.*: 'Improvement in robustness and recognizability of RCS response of U-shaped strip-based chipless RFID tags', *IEEE Antennas Wirel. Propag. Lett.*, 2016, **15**, pp. 2000–2003
[16] Shao, B., Chen, Q., Amin, Y., *et al.*: 'An ultra-low-cost RFID tag with 1.67 Gbps data rate by ink-jet printing on paper substrate'. Asian Solid State Circuits Conf. (A-SSCC), Beijing, China, 2010, pp. 1–4
[17] Jalaly, I., Robertson, I.: 'Capacitively-tuned split microstrip resonators for RFID barcodes'. European Microwave Conf., Paris, France, vol. 2, 2005
[18] Manteghi, M., Rahmat-Samii, Y.: 'Frequency notched UWB elliptical dipole tag with multi-bit data scattering properties'. Antennas and Propagation Society Int. Symp., Honolulu, HI, USA, 2007, pp. 789–792
[19] McVay, J., Hoorfar, A., Engheta, N.: 'Space-filling curve RFID tags'. Radio and Wireless Symp., San Diego, CA, USA, 2006, pp. 199–202
[20] Balbin, I., Karmakar, N.C.: 'Phase-encoded chipless RFID transponder for large-scale low-cost applications', *IEEE Microw. Wirel. Compon. Lett.*, 2009, **19**, (8), pp. 509–511
[21] Islam, M.A., Karmakar, N.C.: 'A novel compact printable dual-polarized chipless RFID system', *IEEE Trans. Microw. Theory Tech.*, 2012, **60**, (7), pp. 2142–2151
[22] Vena, A., Perret, E., Tedjini, S.: 'Chipless RFID tag using hybrid coding technique', *IEEE Trans. Microw. Theory Tech.*, 2011, **59**, (12), pp. 3356–3364
[23] Issa, K., Ashraf, M.A., AlShareef, M.R., *et al.*: 'A novel l-shape ultra wideband chipless radio-frequency identification tag', *Int. J. Antennas Propag.*, 2017, **2017**, article ID 2823565
[24] Dissanayake, T., Esselle, K.P.: 'Prediction of the notch frequency of slot loaded printed UWB antennas', *IEEE Trans. Antennas Propag.*, 2007, **55**, (11), pp. 3320–3325
[25] Constantine, A.B.: 'Microstrip antennas' in '*Antenna theory: analysis and design*' (John Wiley & Sons, 2005, 3rd edn.)
[26] Borkar, V., Ghosh, A., Singh, R., *et al.*: 'Radar cross-section measurement techniques', *Def. Sci. J.*, 2010, **60**, (2), p. 204
[27] Sharma, V., Vithalkar, A., Hashmi, M.: 'Lightweight security protocol for chipless RFID in internet of things (IoT) applications'. 10th Int. Conf. on Communication Systems Networks (COMSNETS), Bangalore, India, January 2018, pp. 468–471
[28] Sharma, V., Vithalkar, A., Hashmi, M.: 'Power saving method in chipless RFID reader for IoT applications'. IEEE Asia-Pacific Conf. on Antennas and Propagation (APCAP), Auckland, New Zealand, August 2018, pp. 374–375
[29] Hartmann, C.S.: 'A global saw ID tag with large data capacity', 2002 IEEE Ultrasonics Symp., 2002. Proc., Munich, Germany, October 2002, vol. 1, pp. 65–69
[30] Vena, A., Perret, E., Tedjini, S.: 'Design of compact and auto-compensated single-layer chipless RFID tag', *IEEE Trans. Microw. Theory Tech.*, 2012, **60**, (9), pp. 2913–2924
[31] Khan, M.M., Tahir, F.A., Farooqui, M.F., *et al.*: '3.56 bits/cm^2 compact inkjet printed and application specific chipless RFID tag', *IEEE Antennas Wirel. Propag. Lett.*, 2016, **15**, pp. 1109–1112
[32] Vena, A., Perret, E., Tedjini, S., *et al.*: 'Design of chipless RFID tags printed on paper by flexography', *IEEE Trans. Antennas Propag.*, 2013, **61**, (12), pp. 5868–5877
[33] Vena, A., P., E., Tedjini, S.: 'A fully printable chipless RFID tag with detuning correction technique', *IEEE Microw. Wirel. Compon. Lett.*, 2012, **22**, (4), pp. 209–211